Communication

Guest-Dependent High Pressure Phenomena in a Nanoporous Metal#Organic Framework Material

Karena W. Chapman, Gregory J. Halder, and Peter J. Chupas

J. Am. Chem. Soc., **2008**, 130 (32), 10524-10526 • DOI: 10.1021/ja804079z • Publication Date (Web): 18 July 2008

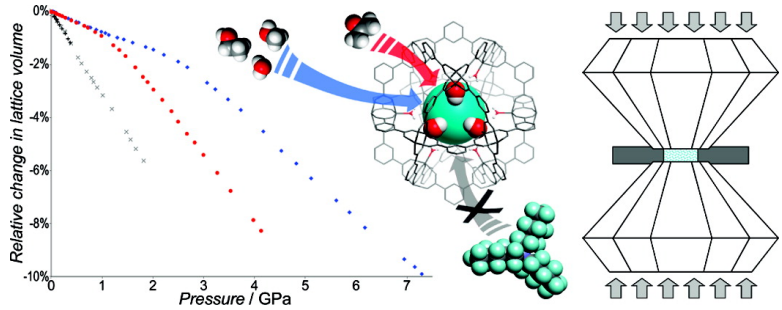

More About This Article

Additional resources and features associated with this article are available within the HTML version:

- Supporting Information
- Links to the 3 articles that cite this article, as of the time of this article download
- Access to high resolution figures
- Links to articles and content related to this article
- Copyright permission to reproduce figures and/or text from this article

View the Full Text HTML

J|A|C|S
COMMUNICATIONS

Published on Web 07/18/2008

Guest-Dependent High Pressure Phenomena in a Nanoporous Metal−Organic Framework Material

Karena W. Chapman,*,† Gregory J. Halder,‡ and Peter J. Chupas†

X-ray Science Division, Advanced Photon Source, Argonne National Laboratory, Argonne, Il, 60439, and Materials Science Division, Argonne National Laboratory, Argonne, Il, 60439

Received May 30, 2008; E-mail: chapmank@aps.anl.gov

Nanoporous metal−organic framework (MOF) materials display a wide range of functional properties with important technological, industrial, and environmental applications in areas such as molecular sensing and strategic gas storage/separation.[1−6] Their well documented structural complexities can be expected to yield unprecedented pressure-induced phenomena, with the further potential for coupling of the host−guest properties afforded by their open structures[2−6] and the small molecule pressure-transmitting fluids often used in high-pressure science. Moreover, compared to traditional solid state materials these open (i.e., low density) systems are likely to be "soft",[7,8] with perturbations to the structure and functionality at less extreme pressures: pressures such as may be routinely encountered in practical applications. For example, densification of polycrystalline porous MOF materials to optimize volumetric gas storage capacity through sample compression (up to several GPa) may distort the framework and pore structure, and accordingly may significantly alter the guest sorption properties (e.g., selectivity). Accordingly, understanding the impact of pressure on MOF systems is of pivotal importance. Here, we report the anomalous high pressure behavior of the nanoporous MOF material Cu_3(1,3,5-benzenetricarboxylate)$_2(H_2O)_3$•{guest}$_9$ (**Cu-btc**) that is associated with the hyperfilling of the pore network. This behavior involves a dramatic transition between a hard regime, where the pressure-transmitting fluid penetrates the framework cavities, and a soft regime, where the guest-framework system compresses concertedly.

As one of the classic MOF systems, the functional properties of **Cu-btc**, including the robust porosity, guest- and ligand-exchange, hydrogen storage, and catalytic behavior, have been widely explored.[9−13] In the **Cu-btc** framework, pairs of Cu^{II} ions, bridged by four carboxylate (μ_2-OCO) groups on discrete 1,3,5-benzenetricarboxylate (btc) ligands, form Cu^{II} dimers (square planar connectivity) which are linked via the trigonal btc molecules to form an extended three-dimensional network with cubic symmetry ($Fm\bar{3}m$, a = 26.4 Å).[9] The rigidity of these components imparts stability to the framework structure which is retained upon reversible removal or exchange of noncoordinated guest species contained within pores in the material as well as nonbridging ligands coordinated axially at the Cu^{II} dimer.[11−13] The three-dimensional pore network is formed by three types of cavities: an alternating (NaCl-type) array of two distinct cuboctahedral cavities with smaller "interstitial" octahedral cavities (Figure 1). As prepared, this pore network contains guest ethanol and water molecules.

A pulverized sample of as-prepared **Cu-btc** was loaded in the hole of a preindented stainless steel foil gasket within a diamond anvil cell (DAC). Polycrystalline quartz was included as an internal pressure marker.[14] The DAC was closed without pressure-transmitting fluid or with methanol−ethanol−water (MEW, 16:3:1 by volume), isopropyl alcohol, or Fluorinert (FC-70, perfluorotri-*N*-pentylamine) to mediate hydrostatic sample compression. In-situ high-pressure diffraction data were collected using the monochromatic X-rays (20.02 keV, 0.61915 Å) available at the 1-BM beamline at the Advanced Photon Source, Argonne National Laboratory in combination with a MAR-345 image plate detector. Sample pressures were varied in the range 0−8 GPa, and within the hydrostatic limit of the fluid for the alcohol-based media. In the standard variable-pressure experiment, single 60 s exposures (3 min per image including experimental overhead) were acquired at each pressure. Five images were accumulated at each pressure for "slow compression" experiments. The raw images were processed within Fit-2D.[15,16] The pressure-dependent lattice parameters were extracted from Le Bail fits to the diffraction data within GSAS.[17,18]

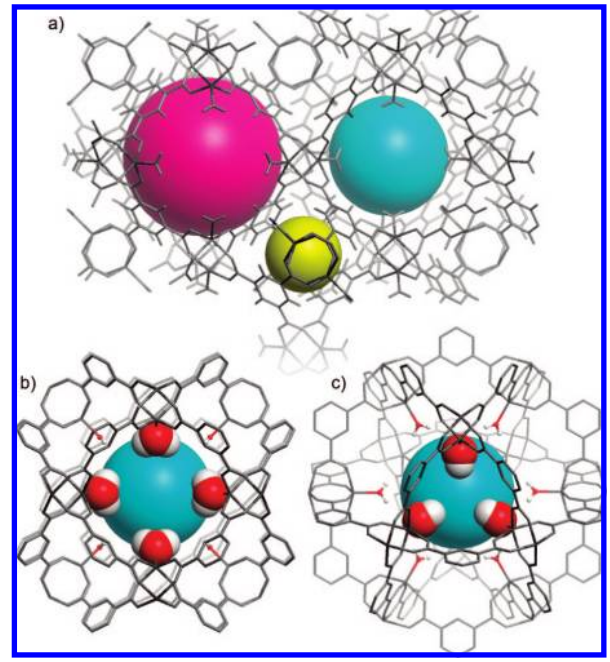

Figure 1. (a) A representation of the **Cu-btc** framework highlighting the distinct guest-accessible cavities at (0,0,0) (pink, ∼11.2 Å diameter), ($^1/_2$, $^1/_2$, $^1/_2$) (blue, ∼8.4 Å diameter), and ($^1/_4$, $^1/_4$, $^1/_4$) (yellow, ∼5.4 Å diameter). The cavities are connected via the ($^1/_2$, $^1/_2$, $^1/_2$) pore through the coordinated water-lined (b) square and (c) triangular apertures, viewed down the (100)- and (111)-directions, respectively. Spheres indicate the approximate volume available to guest molecules (which have been omitted for clarity).

In small molecule alcohol-based pressure-transmitting fluids, the **Cu-btc** framework exhibits a clear transition between two distinct regions of near linear compressibility: appearing quite incompressible at low pressure before compressing rapidly beyond a threshold

† X-ray Science Division.
‡ Materials Science Division.

10.1021/ja804079z CCC: $40.75

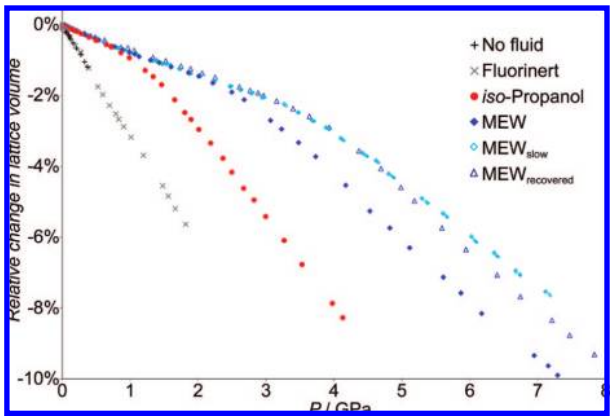

Figure 2. The pressure-induced changes in lattice volume for the **Cu-btc** framework. Errors are within the size of the data points.

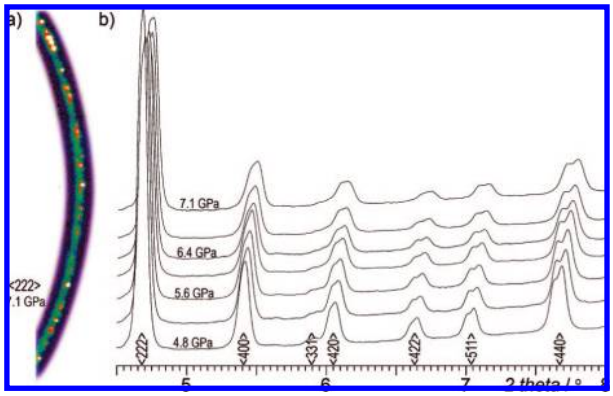

Figure 3. (a) Part of the ⟨222⟩ diffraction ring after slow compression in MEW; (b) peak splitting evident in the diffraction pattern beyond the compressibility transition reflects the different lattice volumes and compressibilities of large single-crystal domains compared to smaller particles.

pressure (Figure 2). The transition was not accompanied by any change in space group symmetry or notable variation in peak intensities. No such transition was apparent without fluid or in large molecule Fluorinert fluid, with rapid, near linear framework compression comparable to the higher pressure, soft regime in alcohol-based fluid. The compressibility transition pressure was strongly dependent on the fluid and occurred at lower pressure in isopropyl alcohol (∼0.8 GPa) compared to MEW (∼2.2 GPa) using similar experimental protocols. It was also dependent on the rate at which pressure was applied and shifted to higher pressure (∼3.3 GPa in MEW) in a slow compression experiment where the sample was held at each pressure for a factor of 5 longer (15 min cf. 3 min).

In MEW, the diffraction peaks broadened progressively beyond the compressibility transition. This was most pronounced for slow compression, where uniform peak splitting could be resolved (Figure 3). Features in the diffraction images suggested that the splitting was due to contributions from two related components, rather than a single lower symmetry phase. The component with a larger lattice volume (at lower diffraction angle) appeared as a continuous diffraction ring from a finely divided powder. The component with a smaller lattice volume (at higher diffraction angle) contributed distinct single-crystal reflections from larger grains within the polycrystalline sample. The different lattice volumes reflect the different compressibilities of these components with a reduced compressibility for the smaller particles.

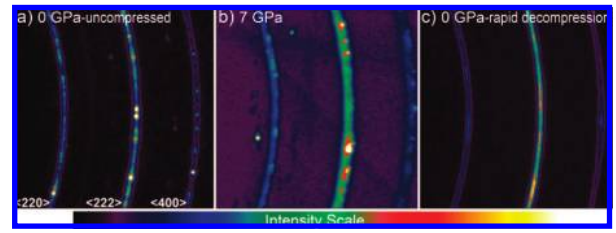

Figure 4. Regions of the diffraction images in MEW for (a) the sample as loaded, (b) at high pressure, and (c) following rapid decompression showing the increased distribution of grain orientations.

Table 1. Bulk Moduli (K) in Different Fluid Media

fluid media	P_{trans} [a] (GPa)	K_{hard} (GPa)	K_{soft} (GPa)
none			30.7(5)[b]
fluorinert			29.5(7)[b]
isopropyl alcohol	∼0.8	117.6(13)[b]	25.9(5)
MEW	∼2.2	116.0(32)[b]	33.6(5)
MEW_{slow}	∼3.3	114.5(17)[b]	41.9(4)[c]
$MEW_{recovered}$	∼3.6	134.4(23)[b]	32.54(23)

[a] P_{trans} is the compressibility transition pressure extrapolated from fits to the hard and soft regimes. [b] Based on fits to data in the pressure range 0−0.5 GPa. [c] Based on average fit to two component region.

Although the original lattice volume and crystalline diffraction were recovered upon release of the pressure, changes in sample morphology were evident depending on the rate of pressure release. With a gradual (i.e., stepwise) release of pressure, the distinct reflections from large single-crystal grains, which persist at high pressure, were retained. However, rapid direct pressure release produced a smearing of the intensity around the diffraction rings reflecting an increased distribution of sample grain orientations and, accordingly, a reduction in average particle size (Figure 4). Variable-pressure compression data collected for a sample previously recovered in this way, showed the compressibility transition to be shifted to higher pressure (∼3.6 GPa in MEW).

The bulk moduli ($K = 1/\beta = -V(\partial P/\partial V)$ where β is the compressibility) obtained from second-order Birch−Murnaghan equations of state fit to the pressure-induced changes in lattice volume, are given in Table 1.

The extreme, intrinsic compressibility measured in the absence of fluid, and the reversibility of this compression, suggests the existence of low energy lattice distortions in the **Cu-btc** framework which are accessed at pressure. The close agreement between data obtained without fluid and upon hydrostatic compression in Fluorinert (which is too large to enter the pores) confirms that this behavior is not an artifact associated with nonhydrostatic effects. The framework compressibility is comparable to that of ionic solids such as NaCl ($K_{NaCl} = 24.4$ GPa)[19] which is itself used as a soft, quasi-hydrostatic medium for higher pressure experiments.

The different high-pressure behaviors evident in the alcohol-based fluid media can be attributed to the interaction of the small fluid molecules with the three-dimensional pore network defined by the framework. The progressive inclusion of extra guests beyond saturation—a pressure-induced hyperfilling or hypersaturation of the pores—underlies the substantially reduced initial compressibility. No framework distortion appears necessary to admit additional guests, with no threshold pressure associated with the hyperfilling. The increased pore occupancy raises the effective internal pressure exerted by guests on the framework, reducing the difference between the internal and external forces on the framework and, thereby, mitigating the effect of increasing applied pressure on the framework compression.

Correspondingly, the abrupt increase in framework compressibility at higher pressures is attributed to a reduced rate of guest inclusion. Beyond a threshold pressure, the framework and accordingly the apertures linking pore cavities are constricted to a critical limit where the guest transmission becomes sterically hindered (possibly involving a "gating" mechanism, with dynamic dilations of the aperture through vibrations/rotations of the defining water molecules and lattice flexing). This pressure depends on the size of the guest and occurs at lower pressure (i.e., compression) for larger molecules such as isopropyl alcohol compared to methanol, ethanol, or water. In fluid mixtures, one might expect the threshold pressure to ultimately relate to the smallest component, with size selective guest inclusion possible within certain pressure-ranges. It may be possible to further tune selectivity by replacing the coordinated water ligands, which define the apertures linking cavities, by other ligands. The general mobility of guests within the individual cavities may also play a role.

The observed particle-size dependence, compression-rate dependence, and pressure-release effects can also be linked to the finite mobility of guests within the crystal grains. For small particles, with shorter diffusion paths through the crystal, and for slower compression experiments, where guests can travel further, the equilibrium loading can be reached and the compressibility transition is shifted to higher pressures. The limited egress of guests upon rapid pressure release leads to excess internal pressure which ruptures crystal grains thereby decreasing particle size and increasing the distribution of particle orientations.

In the soft regime, where the framework and any contained guests compress together without changes to the system composition, the compressibility seems remarkably tolerant to the quantity and type of guest in the pores. This suggests that the contained guests offer little resistance to the compression of the surrounding framework, which is consistent with the low bulk moduli of the neat fluids ($K \approx 1-2$ GPa). As such, the compression behavior of the vacant $Cu_3(btc)_2$ framework—the desolvated **Cu-btc** analogue—would be expected to be similar to that of the guest-loaded framework: $K \approx 30$ GPa. The compressibility in the hard regime, where additional guests are forced into the framework, seems independent of the type of guest and the rate of compression (although a particle size dependence was evident) and, thus, appears to be largely intrinsic to the framework itself.

Notable distinctions are evident between the high pressure behavior of the **Cu-btc** MOF and that of nanoporous zeolites. Zeolites have also shown reduced apparent compressibilities associated with hyperfilling of the pores,[20–22] and for siliceous zeolite Y a comparable hard-to-soft transition; however, the observed compression rates are strongly dependent on the properties (i.e., size) of the guest[20] and the pore occupancy[22]—factors which do not impact the compression rate of the **Cu-btc** system. This may be due to the lower relative flexibility of the linkages in the **Cu-btc** MOF in which, like for mesoporous silicas,[23] the nanoscale architecture of the framework walls plays a determining role in the high pressure behavior.

In conclusion, we have demonstrated that pressure offers a unique and hitherto unexplored means to systematically investigate the often complex structure−function relationships of MOF systems. Their porous nature contributes an additional dimension to the high-pressure behavior which, in the case of **Cu-btc**, results in a duality of compressibility that is triggered by the availability of potential guests and is correlated to the size and penetrability of the guest molecules. The pronounced framework flexing in the soft regime achieves compressibilities comparable to ionic solids such as NaCl, while for the hard regime the material is a factor of 4 less compressible, mimicking compressibilities found in hard metals. The sensitivity of the high-pressure behavior further highlights the profound effect that even moderate pressures, such as those that may be reached during densification or high pressure loadings for gas storage/separation applications, can have on the structural properties of MOFs. Indeed, we envisage that the fundamental understanding of high-pressure phenomena in MOFs will play a pivotal role in the advancement of their diverse applied functionalities.

Acknowledgment. Work performed at Argonne National Laboratory and use of the Advanced Photon Source was supported by the U.S. Department of Energy, Office of Science, Office of Basic Energy Sciences, under Contract No. DE-AC02-06CH11357. Portions of the diamond anvil cell preparation were performed at GeoSoilEnviroCARS (Sector 13), Advanced Photon Source, Argonne National Laboratory. GeoSoilEnviroCARS is supported by the National Science Foundation, Earth Sciences (EAR-0622171), and Department of Energy, Geosciences (DE-FG02-94ER14466). We thank P. L. Lee for beamline support.

Supporting Information Available: Details of sample preparation, diffraction experiments, diffraction data, Le Bail analyses, and equation of state fits. This material is available free of charge via the Internet at http://pubs.acs.org.

References

(1) Hoskins, B. F.; Robson, R. *J. Am. Chem. Soc.* **1990**, *112*, 1546–1554.
(2) Eddaoudi, M.; Kim, J.; Rosi, N.; Vodak, D.; Wachter, J.; O'Keefe, M.; Yaghi, O. M. *Science (Washington, D. C.)* **2002**, *295*, 469–472.
(3) Kitagawa, S.; Kitaura, R.; Noro, S. *Angew. Chem., Int. Ed.* **2004**, *43*, 2334–2375.
(4) Kepert, C. J. *Chem. Commun.* **2006**, 695–700.
(5) Mueller, U.; Schubert, M.; Teich, F.; Puetter, H.; Schierle-Arndt, K.; Pastre, J. *J. Mater. Chem.* **2006**, *16*, 626–636.
(6) Lin, X.; Jia, J. H.; Hubberstey, P.; Schroder, M.; Champness, N. R. *CrystEngComm* **2007**, *9*, 438–448.
(7) Hazen, R. M.; Prewitt, C. T. *Am. Mineral.* **1977**, *62*, 309–315.
(8) Grochala, W.; Hoffmann, R.; Feng, J.; Ashcroft, N. W. *Angew. Chem., Int. Ed.* **2007**, *46*, 3620–3642.
(9) Chui, S. S. Y.; Lo, S. M. F.; Charmant, J. P. H.; Orpen, A. G.; Williams, I. D. *Science (Washington, D.C.)* **1999**, *283*, 1148–1150.
(10) Zhang, X. X.; Chui, S. S. Y.; Williams, I. D. *J. Appl. Phys.* **2000**, *87*, 6007–6009.
(11) Vishnyakov, A.; Ravikovitch, P. I.; Neimark, A. V.; Bulow, M.; Wang, Q. M. *Nano Lett.* **2003**, *3*, 713–718.
(12) Prestipino, C.; Regli, L.; Vitillo, J. G.; Bonino, F.; Damin, A.; Lamberti, C.; Zecchina, A.; Solari, P. L.; Kongshaug, K. O.; Bordiga, S. *Chem. Mater.* **2006**, *18*, 1337–1346.
(13) Peterson, V. K.; Liu, Y.; Brown, C. M.; Kepert, C. J. *J. Am. Chem. Soc.* **2006**, *128*, 15578–15579.
(14) Angel, R. J.; Allan, D. R.; Milletich, R.; Finger, L. W. *J. Appl. Crystallogr.* **1997**, *30*, 461–466.
(15) Hammersley, A. P. ESRF Internal Report 1997, ESRF97HA02T.
(16) Hammersley, A. P.; Svensson, S. O.; Hanfland, M.; Fitch, A. N.; Häusermann, D. *High Pressure Res* **1996**, *14*, 235–248.
(17) Larson, A. C.; Von Dreele, R. B., General Structure Analysis System (GSAS) 2000. *Los Alamos National Laboratory Report, LAUR 86-748*; Los Alamos National Laboratory: NM, 2000.
(18) Toby, B. H. *J. Appl. Crystallogr.* **2001**, *34*, 210–213.
(19) Decker, D. L. *J. Appl. Phys.* **1971**, *42*, 3239–3244.
(20) (a) Hazen, R. M.; Finger, L. W. *J. Appl. Phys.* **1984**, *56*, 1838–1840. (b) Hazen, R. M. *Science (Washington, D.C.)* **1983**, *219*, 1065–1067.
(21) Lee, Y.; Vogt, T.; Hriljac, J. A.; Parise, J. B.; Hanson, J. C.; Kim, S. J. *Nature* **2002**, *420*, 485–489.
(22) (a) Colligan, M.; Forster, P. M.; Cheetham, A. K.; Lee, Y.; Vogt, T.; Hriljac, J. A. *J. Am. Chem. Soc.* **2004**, *126*, 12015–12022. (b) Hriljac, J. A. *Cryst. Rev.* **2006**, *12*, 181–193.
(23) (a) Wu, J. J.; Liu, X. Y.; Tolbert, S. H. *J. Phys. Chem. B* **2000**, *104*, 11837–11841. (b) Wu, J. J.; Abu-Omar, M. M.; Tolbert, S. H. *Nano Lett.* **2001**, *1*, 27–31.

JA804079Z